

## **2 Interaction of Intense Electromagnetic Fields with Hot Dense Plasma**

The physical effects investigated in this work are all based on the interaction between ultrashort laser pulses and the plasma created on the surface of a liquid target. This is demonstrated in Chapter 4 where  $K_{\alpha}$  line radiation is generated using an ultra short laser pulse and a gallium target. Chapter 6 examines the energy of electrons and protons accelerated out of a water jet target. In Chapter 2 the necessary definitions are given and processes are discussed that lead to such effects, starting with basic plasma theory and a description of methods usually applied to calculate plasma processes, followed by a discussion of the absorption processes in strong or ultra-strong laser fields. This topic became very important with the rapid development of short-pulse high-power lasers which allows today for the generation of ultrashort X-ray pulses in a table top-setup [MKR91]. Following the discussion of light absorption processes, the emission of line and broadband radiation in the hard X-ray range is considered.

A final section of this chapter deals with the particle-acceleration mechanisms in and beyond laser-produced plasmas. This topic is closely related to the interaction between laser light and instabilities within the plasma. This section focuses on two aspects: (1) plasma waves and resonant interactions between these waves and the laser light, (2) particular effects, which were found to be responsible for the acceleration of the much heavier protons.

### ***2.1 Introduction to Plasma Physics***

Our daily experience is dominated by three states of matter: Solid, liquid and gas. But in the universe the fourth state, the plasma, is dominant (aside from black holes). This fourth state consists basically of charged particles (electrons and ions) and it can be found in the interstellar space as well as in the stars (Fig. 2-1). As an example, the hydrogen plasma in the core of the sun has a temperature of about  $10^7$  K, an electron density of  $10^{25}$   $\text{cm}^{-3}$  and a pressure of  $10^9$  bar ([GKV89],[UMS01]). In this case, the plasma is hot and dense enough to fuel the process of nuclear fusion. Since the advent of nuclear power plants (and bombs),

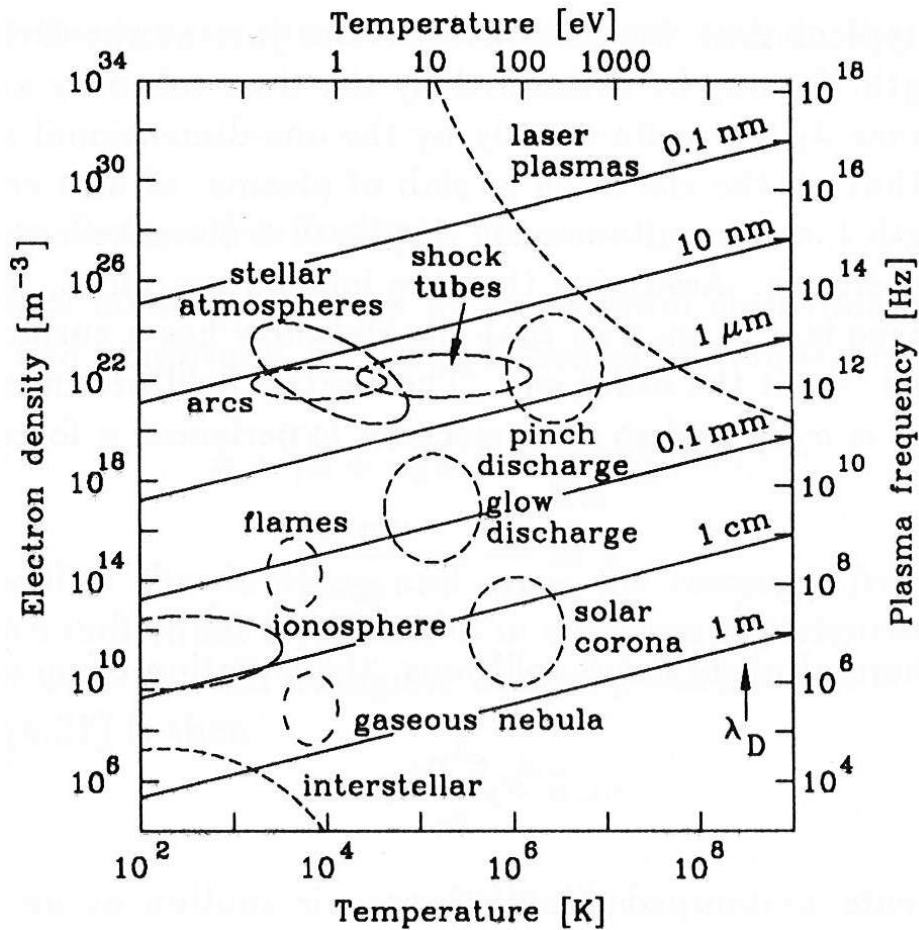


Fig. 2-1 : Different types of plasma in nature and science [MB93]. The tilted lines denote the Debye length.

using nuclear fusion instead of fission for energy production has been subject to scientific investigation and reasoning too. This led to an enormous progress in plasma physics as well as in laser physics in the last decades (see e.g. [KRU88]). The basic idea was to focus an ultra-intense laser pulse onto a small target in order to start the ignition of a fusion target (“fast ignitor” approach [TAB94]). For such experiments laser systems with up to  $10^{21}$  W/cm<sup>2</sup> focused irradiance were developed [PPS99]. Beside the research on the field of laser fusion, such tools opened up extensive research on laser produced plasma. It became possible already in the 1980s to study hot and dense plasma not only in the spectra of remote stars but also in a laser laboratory.

### 2.1.1 Basic Parameters

As already indicated in Fig. 2-1, conventionally one uses two parameters to describe a plasma: Temperature and electron density. The temperature in plasma physics is often expressed in eV, giving the energy equivalent of the temperature with the Boltzmann constant

$k_B T$  ( $k_B = 8.617 \times 10^{-5}$  eV/K). Another important plasma parameter is the *Debye length*  $\lambda_D$  (see, e.g., Attwood [ATT99] or Michette and Buckley [MB93]):

$$\lambda_D = \left( \frac{\epsilon_0 k_B T_e}{e^2 n_e} \right)^{1/2}, \quad / 2-1$$

where  $\epsilon_0$  is the electric constant (permittivity of free space),  $k_B$  is the Boltzmann constant,  $T_e$  is the electron temperature,  $e$  is the elementary charge and  $n_e$  the electron density. The Debye length denotes a distance beyond which the potential of an individual charge is shielded by surrounding mobile charges. That implies, that on spatial scales shorter than  $\lambda_D$  the presence and effects of individual charges are evident. On a scale larger than  $\lambda_D$ , charged particle interactions tend to occur through collective motions, such as electron- and ion-acoustic waves. One can also use this concept to separate the behavior of the charges into *collisional* (spatial scale  $\ll \lambda_D$ , binary collisions dominate the interaction) and *collective* (spatial scale  $\gg \lambda_D$ , plasma is quasi-neutral, collective behavior dominates). The Debye lengths of typical plasmas can be found in Fig. 2-1. It should be mentioned that a detailed theory of the shielding of electric fields in plasma is similar to the Debye-Hückel theory in electrolytes (see e.g. [GKV89]).

A parameter of particular importance for the interaction between electromagnetic fields and plasma is the plasma frequency  $\omega_p$ . The plasma frequency is the resonance frequency for collective oscillations of the electrons about their equilibrium positions:

$$\omega_p = \left( \frac{e^2 n_e}{\epsilon_0 m_e} \right)^{1/2}. \quad / 2-2$$

Here,  $m_e$  denotes the electron mass and  $n_e$  the electron density. The plasma frequency can be seen as the inverse of the typical time for collective action, just as the Debye length is the typical length.

When a laser pulse impinges normally onto a solid target it creates with its pre-pulse or leading edge a pre-plasma with an increasing electron density towards the solid body. Therefore it is appropriate for the understanding of interaction processes between the laser pulse and the target surface to assume an electron density gradient as indicated in Fig. 2-2<sup>1</sup>. The steepness of such a profile depends on the temporal laser pulse contrast. An electromagnetic wave with frequency  $\omega_L \gg \omega_p$  can penetrate into the plasma and interacts with a medium of resonance frequency  $\omega_p$ . The electrons within the plasma can not follow the

---

<sup>1</sup> For a first discussion of the interaction between electromagnetic radiation and the plasma, it is sufficient to consider only the movement of the electrons because ions are almost immobile at these high frequencies.

## 2 Interaction of Intense Electromagnetic Fields with Hot Dense Plasma

rapid oscillation and the wave propagates (Fig. 2-2 a). The laser beam can only penetrate into the target up to a point, where the plasma frequency  $\omega_p$  equals the frequency of the wave  $\omega_L$ . The corresponding density at this point is called critical density  $n_{crit}$  and can be calculated ( $\omega_p = \omega_L$ ) from equation /2-2/:

$$n_{crit} = \frac{\omega_L^2 \epsilon_0 m_e}{e^2} , \quad /2-3$$

or, in terms of the wavelength (in microns),

$$n_{crit} = \frac{1.11 \times 10^{21} e/cm^3}{\lambda^2 (\mu m)} . \quad /2-4$$

At the critical density many complex processes occur, but in a simple harmonic oscillation picture, the plasma-electrons are excited at their resonance frequency and absorb a large part of the electromagnetic radiation. Although this picture is strongly simplified, absorption at the so-called *critical surface* (where  $n_e = n_{crit}$ ) is very important for the energy transfer between laser pulses and the plasma. Further propagation into the target beyond the skin depth  $l_s = c/\omega_p$  is impossible. It should be noted that  $n_{crit}$  basically depends on the wavelength of the electromagnetic wave. That is, laser pulses with shorter wavelength can penetrate deeper into a plasma than pulses with a longer wavelength.

On a very steep density gradient, e.g. if no laser pre-pulse is present, it might occur that the wave hits the plasma at a density even greater than  $n_{crit}$  (Fig. 2-2 b). In such an *overdense* plasma the plasma frequency would be much greater than the frequency of the wave:  $\omega_p \gg \omega_L$ . The electrons could move quickly enough to cancel the disturbance, and the wave would not propagate further. The absorption is lower than at the resonance frequency and part of the radiation is (back) scattered.

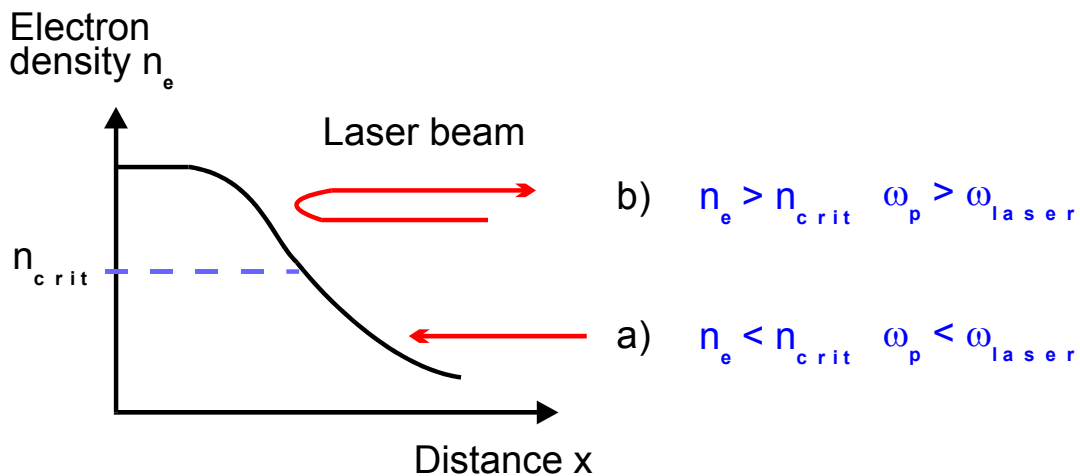


Fig. 2-2 : Simplified scheme of laser plasma interaction for a) underdense and b) overdense plasma.

The physical picture is also evident from the refractive index  $n$  in plasma for a transversal electromagnetic wave with frequency  $\omega_L$  (e.g. [ATT99]):

$$n = \sqrt{1 - \frac{\omega_p^2}{\omega_L^2}} \quad , \quad / 2-5$$

or equivalently:

$$n = \sqrt{1 - \frac{n_e}{n_{crit}}} \quad . \quad / 2-6$$

For  $n_e < n_{crit}$  the index of refraction is real and smaller than 1. Beyond the so called *critical surface* (where  $n_e > n_{crit}$ ),  $n$  becomes imaginary.

So far some basic phenomena of laser plasma interaction have been introduced. A more detailed discussion of absorption (section 2.2) or emission processes (section 2.3) follows in the next sections.

### 2.1.2 Microscopic, Kinetic, and Fluid Descriptions of a Plasma

Models for the theoretical description of a plasma can be found in various textbooks (e.g. [ATT99], [KRU88], [HM79]). The main difference between these models are the complexity of the information about the location and velocity of the individual particles and the theoretical methods they apply. Some are very detailed but mathematically intractable. Others simplify the  $(\mathbf{r}, \mathbf{v})$  distribution and consider only collective motions instead of tracking all individual particles. In the following section three ways for the theoretical description of plasmas with increasing degree of simplification in the velocity distribution are introduced.

#### The microscopic description

The most general approach suggested by Klimontovitch [KLI67] starts with a microscopic distribution function describing the position and the velocity of all particles in a six dimensional phase space:

$$f(\mathbf{v}, \mathbf{r}; t) = \sum_{i=1}^N \delta[\mathbf{r} - \mathbf{r}_i(t)] \delta[\mathbf{v} - \mathbf{v}_i(t)] \quad . \quad / 2-7$$

Here  $\mathbf{r}_i(t)$  and  $\mathbf{v}_i(t)$  describe the motion of the  $i$ th particle. Taking the time derivative of this function and introducing the Lorentz force (for the term  $\partial \mathbf{v}_i / \partial t$ ) leads to the so called *Klimontovich equation* which describes the temporal evolution of the microscopic distribution function  $f(\mathbf{v}, \mathbf{r}; t)$  in the phase space:

## 2 Interaction of Intense Electromagnetic Fields with Hot Dense Plasma

---

$$\frac{\partial f}{\partial t} + \mathbf{v} \cdot \nabla f + \frac{q}{m} (\mathbf{E} + \mathbf{v} \times \mathbf{B}) \cdot \nabla_v f = 0 \quad . \quad / 2-8$$

To get a set of self-consistent field equations the charge density  $\rho$  and the current  $\mathbf{J}$  are introduced in terms of distribution functions  $f_j(\mathbf{r}, \mathbf{v}; t)$  for different types of particles (e.g.  $j=1$  for electrons and  $j=2$  for ions):

$$\rho_j(\mathbf{r}, t) = q_j \int f_j(\mathbf{v}, \mathbf{r}; t) d\mathbf{v} \quad / 2-9$$

$$\mathbf{J}_j(\mathbf{r}, t) = q_j \int \mathbf{v} f_j(\mathbf{v}, \mathbf{r}; t) d\mathbf{v} \quad . \quad / 2-10$$

This can be introduced into Maxwell's equations, leading to a set of self –consistent field equations (*Maxwell-Klimontovitch equations*) describing the plasma dynamics on the microscopic level.

$$\begin{aligned} \nabla \times \mathbf{H} &= \frac{\partial \mathbf{D}}{\partial t} + \sum_j q_j \int \mathbf{v} f_j(\mathbf{v}, \mathbf{r}; t) d\mathbf{v} \\ \nabla \times \mathbf{E} &= -\frac{\partial \mathbf{B}}{\partial t} \\ \nabla \cdot \mathbf{D} &= \sum_j q_j \int f_j(\mathbf{v}, \mathbf{r}; t) d\mathbf{v} \\ \nabla \cdot \mathbf{B} &= 0 \end{aligned} \quad / 2-11$$

Including all particle species the Klimontovich equation finally changes to:

$$\frac{\partial f_j}{\partial t} + \mathbf{v} \cdot \nabla f_j + \frac{q_j}{m_j} (\mathbf{E} + \mathbf{v} \times \mathbf{B}) \cdot \nabla_v f_j = 0 \quad . \quad / 2-12$$

Equations /2-11/ and /2-12/ give a complete description of the plasma behavior. But because of the discrete character of  $f(\mathbf{r}, \mathbf{v}; t)$  it is highly stochastic and varying rapidly over space and time. And it involves the six phase-space parameters of each particle which makes analytical treatment for real plasmas difficult.

### **The kinetic description**

In the kinetic description of the plasma, the distribution function  $f(\mathbf{v}, \mathbf{r}; t)$  is simplified. It contains no information about the individual particle, it rather represents an average velocity distribution  $f(\mathbf{v})$  with slow space-time dependence. It is averaged over a space, containing a large number of particles. Therefore, from the distribution function  $f(\mathbf{v}, \mathbf{r}; t)$  a slowly varying part ( $\bar{\phantom{x}}$ ) and a fluctuating part ( $\tilde{\phantom{x}}$ ) can be defined:

$$f(\mathbf{v}, \mathbf{r}; t) = \bar{f}(\mathbf{v}, \mathbf{r}; t) + \tilde{f}(\mathbf{v}, \mathbf{r}; t) . \quad / 2-13$$

The fields are written as slow and fluctuating fields too:

$$\mathbf{E}(\mathbf{r}, t) = \bar{\mathbf{E}}(\mathbf{r}, t) + \tilde{\mathbf{E}}(\mathbf{r}, t) . \quad / 2-14$$

Substituting these into the Klimontovich equation /2-12/, and averaging over a spatial scale sufficiently large to give a smoothed kinetic equation for the velocity function, yields:

$$\frac{\partial \bar{f}_j}{\partial t} + \mathbf{v} \cdot \nabla \bar{f}_j + \frac{q_j}{m_j} (\bar{\mathbf{E}} + \mathbf{v} \times \bar{\mathbf{B}}) \cdot \nabla_{\mathbf{v}} \bar{f}_j = - \frac{q_j}{m_j} \nabla_{\mathbf{v}} \cdot (\tilde{\mathbf{E}} + \mathbf{v} \times \tilde{\mathbf{B}}) \tilde{f}_j . \quad / 2-15$$

The right side of the equation is often denoted as *collision* term, because it expresses the microscopic behavior of the particles within a spatial scale in the order of a Debye length, where binary collisions are the dominating form of interaction. In contrast,  $\bar{\mathbf{E}}$  represents the field due to deviations from charge neutrality over larger space scales. This field gives rise to *collective* motion of the charges.

If many electrons are within the range of a Debye length (or, within a *Debye sphere*, a sphere with radius  $\lambda_D$ ), the strongly oscillating microfields of individual particles average to zero and the collective behavior dominates. Thus, for a dense plasma the collisional term can be neglected and the so-called *collisionless Vlasov equation* can be formulated:

$$\frac{\partial \bar{f}_j}{\partial t} + \mathbf{v} \cdot \nabla \bar{f}_j + \frac{q_j}{m_j} (\bar{\mathbf{E}} + \mathbf{v} \times \bar{\mathbf{B}}) \cdot \nabla_{\mathbf{v}} \bar{f}_j \equiv 0 . \quad / 2-16$$

In a similar way one can substitute fields as shown in equation /2-14/ into Maxwell's equations /2-11/, retain only the slow varying quantities and obtain the collisionless Maxwell-Vlasov equations. These equations are similar to /2-11/ in the sense that only the fields like  $\bar{\mathbf{E}}$  and the other slowly varying quantities (  $\bar{\quad}$  ) describe quantities different from those in the microscopic case /2-11/.

The collisionless Vlasov equation can be used, for example, to describe the growth and decay of electron acoustic waves (see section 2.4), the so called Landau growth or damping [LL46].

### **The fluid description**

The kinetic description essentially uses a velocity distribution for the calculation of plasma behavior. In the fluid description a set of fluid-dynamical equations for the description of a plasma is developed with some further simplifications.

## 2 Interaction of Intense Electromagnetic Fields with Hot Dense Plasma

This is done in a two-step mathematical process: First, from the velocity distribution function  $f_j(\mathbf{v}, \mathbf{r}; t)$  several physical quantities are derived, including the particle density  $n_j(\mathbf{r}, t)$  for each species, the average velocity  $\bar{\mathbf{v}}_j(\mathbf{r}, t)$ , the partial pressure  $P_j(\mathbf{r}, t)$  and others. For the derivation of these quantities, the velocity moments<sup>1</sup> of the kinetic velocity distribution function  $f_j(\mathbf{v}, \mathbf{r}; t)$  are written down. For this purpose the distribution function  $f_j(\mathbf{v}, \mathbf{r}; t)$  is multiplied by 1,  $\mathbf{v}$ ,  $\mathbf{v}\mathbf{v}$ , etc. and integrated over  $d\mathbf{v}$ . In a second step this procedure is applied to the collisionless Vlasov equation. Both steps are shown briefly below.

In the first step, the electron density  $n_e$  and the electron average velocity  $\bar{\mathbf{v}}$  are written as moments of  $f_e(\mathbf{v}, \mathbf{r}; t)$ :

$$n_e(\mathbf{r}, t) = \int f_e(\mathbf{v}, \mathbf{r}; t) d\mathbf{v} \quad , \quad / 2-17$$

$$n_e \bar{\mathbf{v}}(\mathbf{r}, t) = \int \mathbf{v} f_e(\mathbf{v}, \mathbf{r}; t) d\mathbf{v} \quad . \quad / 2-18$$

A third moment gives  $\mathbf{P}_e$ , the tensor electron pressure dyadic (a nine-element tensor), continued with the electron thermal (kinetic) energy  $U_e$  and the vector heat flux  $\mathbf{Q}_e$ :

$$\mathbf{P}_e = \frac{1}{2} n_e m \overline{\tilde{\mathbf{v}} \otimes \tilde{\mathbf{v}}} = \int \tilde{\mathbf{v}} \otimes \tilde{\mathbf{v}} f_e(\mathbf{v}, \mathbf{r}; t) d\mathbf{v} \quad , \quad / 2-19$$

$$n_e U_e = \frac{1}{2} n_e m \overline{\tilde{\mathbf{v}}^2} = \int \tilde{\mathbf{v}}^2 f_e(\mathbf{v}, \mathbf{r}; t) d\mathbf{v} \quad , \quad / 2-20$$

$$\mathbf{Q}_e = \frac{1}{2} n_e m \overline{\tilde{\mathbf{v}}^2 \tilde{\mathbf{v}}} = \int \tilde{\mathbf{v}}^2 \tilde{\mathbf{v}} f_e(\mathbf{v}, \mathbf{r}; t) d\mathbf{v} \quad . \quad / 2-21$$

Then, in a second step, equations for these fluid mechanical quantities are derived by calculating the velocity moments of the collisionless Vlasov equation. The first moment of the Vlasov equation is this:

$$\int d\mathbf{v} \left[ \frac{\partial f_j}{\partial t} + \mathbf{v} \cdot \nabla f_j + \frac{q_j}{m_j} (\mathbf{E} + \mathbf{v} \times \mathbf{B}) \cdot \nabla_V f_j \right] = 0 \quad . \quad / 2-22$$

Such integrals can be solved by substituting parts of the integral using the physical quantities connected with the velocity moments of the distribution function  $f(\mathbf{v}, \mathbf{r}, t)$  as demonstrated in

<sup>1</sup> In the simplest case this method calculates the center of gravity of a curve. It can be found in standard engineering text books, e.g. [GOE87].

/2-17/ ... /2-21/. Application of this method to the first moment of the Vlasov equation /2-22/ and appropriate assumptions about the Lorentz force lead to the *continuity equation* for the averaged quantities:

$$\frac{\partial n_e}{\partial t} + \nabla \cdot (n_e \bar{\mathbf{v}}) = 0 \quad . \quad /2-23$$

The second velocity moment of the collisionless Vlasov equation results in the *momentum conservation law*:

$$m \left( \frac{\partial}{\partial t} + \bar{\mathbf{v}} \cdot \nabla \right) \bar{\mathbf{v}} = -\frac{1}{n_e} \nabla P_e - e(\mathbf{E} + \bar{\mathbf{v}} \times \mathbf{B}) \quad . \quad /2-24$$

Here ,  $\mathbf{P}$  is the dyadic tensor of electron pressure (see /2-19/) and reduced to a scalar pressure  $P_e$  for an isotropic distribution function. All these equations have been applied to electrons but they can, of course, be transferred to other particle species.

Multiplication of the Vlasov equation with the (scalar) kinetic energy  $mv^2/2$  leads to

$$\int \frac{m v^2}{2} \left[ \frac{\partial f_j}{\partial t} + \mathbf{v} \cdot \nabla f_j + \frac{q_j}{m_j} (\mathbf{E} + \mathbf{v} \times \mathbf{B}) \cdot \nabla_v f_j \right] d\mathbf{v} = 0 \quad , \quad /2-25$$

which can be transformed into a *conservation of energy* equation:

$$n_j \left( \frac{\partial}{\partial t} + \bar{\mathbf{v}} \cdot \nabla \right) U_j + (\mathbf{P}_j \cdot \nabla) \cdot \mathbf{v} + \nabla \cdot \mathbf{Q}_j = 0 \quad , \quad /2-26$$

where for each species  $U_j$  is the (random) thermal energy (Eq. /2-20/),  $\mathbf{P}$  is the dyadic tensor of electron pressure (Eq. /2-19/) and  $\mathbf{Q}_j$  is the thermal flux vector (Eq. /2-21/). Finally, some rules for the thermodynamic behavior of the plasma can be derived. One is the so-called *adiabatic condition* between partial pressure and density for processes (e.g. wave motions, etc) involving no heat transfer:

$$\frac{P_j}{n_j^\gamma} = const. \quad , \quad /2-27$$

where  $\gamma = 1 + 2/N$ , and  $N$  is the number of degrees of freedom of the particles involved.

The equations for the fluid mechanical quantities /2-23/.../2-27/ together with appropriate forms of Maxwell's equations form a set of equations, the so called *Maxwell-Euler equations*, which describe plasma dynamics on fluid level completely and self-consistently.

## 2 Interaction of Intense Electromagnetic Fields with Hot Dense Plasma

---

So far equations for charged particles on a fluid level have been described. These fluids are also referred to as *charged fluids*. The so called *two-fluid description* includes two fluids of different particle species (typically electrons and ions). In this case one fluid has low viscosity (electrons) while the other is rather inert and moving more slowly (ions), depending on density and temperature. Short-range collisions would lead to a momentum transfer between the different species. These collisions could be accounted for by an appropriate term on the right side of the Vlasov equation [2-16]. In the momentum equation in the fluid description, this term would appear in the form of  $-mf_{ei}\bar{\mathbf{v}}$ , where  $f_{ei}$  is the effective electron-ion collision frequency.

What is the importance of these plasma-description models for this work? At first, in plasma physics most theoretical predictions involve numerical simulations based on one or another way of the plasma-description introduced above. Some simulation methods will be reviewed briefly in the next sub-section. Application of such a method to our experiments will be discussed in section 4.2.4. Another point involves the acceleration processes of particles in a plasma. Electron wave effects in plasmas account for some particular acceleration mechanisms, which can accelerate electrons in a plasma to relativistic energies. The theory of longitudinal and transversal waves in a plasma is, of course, based on the plasma theory, although it is beyond the scope of this work to show that in all details.

### 2.1.3 Numerical Simulation Techniques

Because of the extreme experimental parameters such as short time scales, microscopic dimensions or stellar pressures in the physics of laser produced plasmas, plasma diagnostics is rather difficult. Therefore, numerical simulations represent an essential tool for the understanding of the complex processes within a plasma. Similar to the plasma description methods presented above the numerical methods can be classified into those more particle-oriented and others using more fluid-like models. Here, particle oriented means, that the algorithms use a model such as the microscopic or kinetic description above, where much information about the individual particle is included. The basic approach for such particle codes can be described as follows [KRU88]: From the location and the velocity of a number of particles, the charge and current densities are calculated. Then, using Maxwell's equations, the self consistent electric and magnetic fields can be determined from charge and current densities. As suggested in Fig. 2-3, these fields and the equations of motion can be used to advance the positions and velocities of the charges.

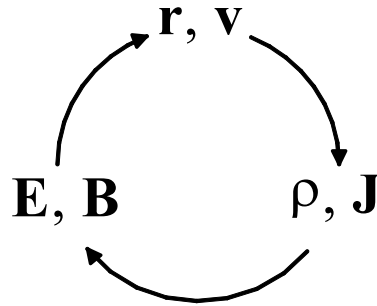


Fig. 2-3: The basic cycle of a particle simulation code [KRU88].

This cycle can be repeated with a temporal resolution small enough to resolve the smallest temporal features (typically the inverse of the plasma frequency). The spatial grid should be small enough to resolve collective motion. This method is rather simple, nevertheless powerful (if sufficient computation power is available) and particularly helpful for the solution of kinetic problems, such as Raman processes in plasmas etc.

Other numerical methods focus on the hydrodynamic models for plasmas. There, quantities such as density, temperature, pressure, vector velocity etc. are traced in their temporal and spatial evolution. In the case of LASNEX [ZK75], a famous code from Lawrence Livermore National Laboratory, the plasma is grouped into zones of specified mass and appropriate fluid-level parameters. The evolution of these fluid parameters is followed then using a Lagrangian calculation.

One code which was used in research connected with the gallium experiments presented in Chapter 4 is ITS [ITS]. ITS permits a state-of-the-art Monte Carlo solution of linear time-integrated coupled electron/photon radiation transport problems with or without the presence of macroscopic electric and magnetic fields of arbitrary spatial dependence. More details on Monte-Carlo calculations can be found, e.g., in chapter 11 of the textbook by Motz [HM79].

Other codes for plasma calculations that should be mentioned (without claiming completeness) are ZOHAR from LLNL [LL76] and MULTI [RSM88] from the MPQ Garching. Specific simulations of accelerated protons can be found, e.g., in the work of Wilks et al. [WLC01], Ruhl et al. [RBC01] and Pukhov [AP01].

2.2 Light Absorption Effects in Dense Plasma

The interaction of strong laser fields with gaseous or solid matter is a field of physics covering a multitude of effects. An overview of such effects in a graph (Fig. 2-4) can be found in a review article by Gibbon and Förster [GIB96]. The axis in this graph is the laser irradiance  $I\lambda^2$ , which is the scaling parameter for most effects in laser-plasma interaction. With the large influence of the laser wavelength in the irradiance, it becomes apparent why many plasma effects, which will be discussed for ultrashort laser pulses at 800 nm, are known for decades from CO<sub>2</sub> lasers at much lower intensity.

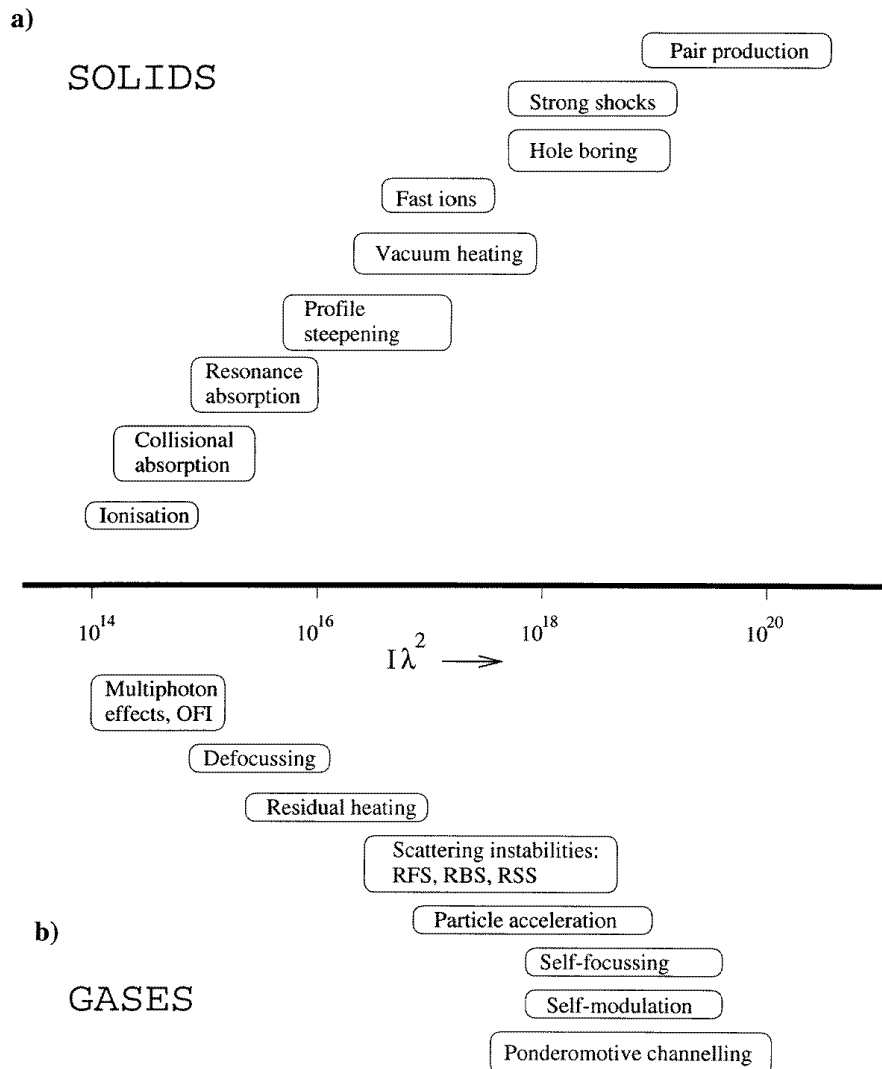


Fig. 2-4: Physics of strong laser-pulse interaction with a) solids and b) gases [GIB96].

The effects in both, solids and gases, are relevant here, because, on one hand, ultrashort laser pulses create steep gradients and high electron densities, comparable to those in solids, when they impinge on liquid targets (as described in Chapter 4). On the other hand, several processes, such as electron acceleration (which is important for X-ray generation as well as for particle acceleration in general), can become efficient in the pre-plasma of lower density, comparable to ionized gases. In the following, some of the main effects in the interaction of strong laser fields with plasmas are introduced. First, we focus on the absorption effects. Subsequent sections deal with radiation emission and wave phenomena in plasmas, respectively.

### 2.2.1 Absorption in Strong Laser Fields

The first effect when a strong electromagnetic field enters a target surface is ionization. Apparently, the energy of a single laser photon at  $\lambda=800$  nm ( $E= 1.55\text{eV}$ ) is too small for ionization of the target material. Therefore, the large amplitude of the light field becomes effective and multiphoton ionization and tunneling processes are dominant. Thus, a plasma with free electrons and ions is created. The free electrons in the plasma can not take over the energy directly from the photons (they can not fulfill the energy and momentum conservation simultaneously), but they oscillate in the electrical field of the light wave. In this oscillation (see equation 2-15) damping through electron–ion collisions occurs. Taking the oscillation of the electron in the electric field  $E$  and adding a collision term  $m_e f_{ei} v$  ( $f_{ei}$  is the electron–ion collision frequency and  $v$  is the electron velocity), the equation of motion for the electron is

$$m_e \frac{\partial v}{\partial t} + m_e f_{ei} v = -eE \quad . \quad / 2-28$$

Thus, a transverse light wave is transmitted in the (underdense) plasma and damped by collisions between electrons and ions. The electrons are accelerated and their oscillatory energy is converted into thermal energy of the plasma particles by collisions with ions. The temperature of the plasma increases. This linear damping mechanism is referred to as *collisional damping*, *collisional absorption* or *inverse bremsstrahlung* (the inverse of the *bremsstrahlung* emission effect, where the electrons are decelerated and photons are emitted). It should be noted, how the electron-ion collision frequency  $f_{ei}$  depends on the plasma ( $n_e$  electron density,  $k_B T_e$  electron thermal energy) and target ( $Z$  ion charge) parameters:

$$f_{ei} \propto \frac{Z n_e}{(k_B T_e)^{3/2}} \quad . \quad / 2-29$$

## 2 Interaction of Intense Electromagnetic Fields with Hot Dense Plasma

---

From this equation one can see that for a hot plasma the absorption is lower and for a dense plasma the damping increases. Furthermore, at least two effects should be mentioned for the absorption in the underdense plasma: First, there is the possibility of plasma waves, coming up from the thermal noise and interacting with the transmitted wave. These phenomena will be discussed later in more detail (section 2.4). Second, because of the density and temperature gradients within the plasma, electromagnetic waves experience a spatial (and temporal) change in the index of refraction. Therefore, the propagation and absorption of light waves in plasma depends strongly on its angle of incidence and the part of radiation, which is refracted away from the plasma, can be very high.

The linear absorption approach in equation /2-28/ is valid as long as the laser energy density is smaller than the thermal energy density. For stronger light fields non-linear terms and parametric processes become relevant. Furthermore the light pressure begins to steepen the electron density profile, which also reduces the role of collisional absorption.

For a steeper plasma gradient another absorption process, the so-called *resonance absorption*, becomes important. Thus a short-range plasma can be created with ultrashort femtosecond high-contrast laser pulses, where expansion is minimized, or, with super-strong nanosecond pulses, where the light pressure  $P_L=2I_L/c$  ( $I_L$  laser intensity) is strong enough to compress any pre-plasma. In the case of such steep density gradients part of the laser radiation can reach the critical surface, where  $\omega_L=\omega_p$ , without being absorbed or refracted. There, further propagation of the electromagnetic wave is impossible. Only the field component of the electromagnetic field parallel to the density gradient (or perpendicular on the critical surface) can accelerate electrons into the critical surface. For normal incidence this field component is zero and for glancing incidence the wave is refracted away from the critical surface. But for a certain angle of incidence, the effect is optimal and many accelerated electrons can tunnel into the denser regions of the plasma. Theoretically, the absorption of laser energy using this effect can peak at about 50% [FKL75]. This can be partially understood by the resonant character of the phenomenon: Because it happens at the critical surface, the laser frequency equals the plasma resonance frequency  $\omega_L=\omega_p$ . Thus, a resonantly (hence *resonance absorption*) driven longitudinal electron wave can be build up on the critical surface and supports the tunneling of the electrons into the overdense plasma regions. In contrast to the collisional absorption processes, this mechanism is also referred to as one of the collisionless absorption processes. The electrons accelerated in this manner can have a kinetic energy much higher than the thermal energy of the plasma. Therefore they are called *hot electrons*. The effects of

deceleration of such hot electrons in the target material lead to the emission of bremsstrahlung as well as characteristic line radiation (see section 2.3). This, in turn, may be used as source of radiation (e.g. monochromatic X-ray source), or as a means to collect information on plasma processes (e.g. bremsstrahlung as a simple means of estimating the kinetic energy of the hot electrons (see Chapter 4)). It should be noted, that these effects, where electron energies of tens or hundreds of keV are measured, could not be due to collisional absorption.

To estimate the conditions under which resonant absorption becomes significant, one can introduce the concept of *quiver velocity* and *quiver energy*. The quiver velocity denotes the velocity component of the plasma electrons due to the electromagnetic field of the laser light. For high laser intensities the oscillation in the electromagnetic field dominates the electron motion and the thermal velocity  $\sqrt{k_B T / m_e}$  is replaced by the quiver velocity  $eE/m_e\omega_L$ . More intriguing is the formulation for the quiver velocity  $v_{os}$  depending on the irradiance  $I\lambda^2$  [GIB96]:

$$v_{os} = 0.84 c \left( \frac{I}{10^{18} \text{ W/cm}^2} \frac{\lambda^2}{\mu\text{m}^2} \right)^{1/2}. \quad / 2-30$$

Thus, for a laser with  $I = 10^{16} \text{ W/cm}^2$  and  $\lambda = 1 \mu\text{m}$  the oscillation or *quiver energy*  $U_{os} = 0.5 m_e v_{os}^2$  is already 1 keV. For such strong laser fields the quiver energy becomes larger than the thermal energy and effects like resonance absorption become effective.

### 2.2.2 Absorption in Ultra-Strong Laser Fields

The classification into strong and ultra-strong laser fields is necessarily somewhat arbitrary. While Brunel in 1987 [BRU87] still put  $I\lambda^2=10^{16} \text{ W } \mu\text{m}^2/\text{cm}^2$  as very-high intensity, today it is more popular to put this limit at  $10^{18} \text{ W } \mu\text{m}^2/\text{cm}^2$ , where the relativistic effects in the plasma become relevant. We will use here the first limit, because some extraordinary absorption phenomena start here. One is described by Brunel as “Not-So-Resonant, Resonant Absorption” [BRU87]. He points out, that at  $I\lambda^2=10^{16} \text{ W } \mu\text{m}^2/\text{cm}^2$  the electron density profile becomes so steep, that the amplitude of the resonant electron plasma wave exceeds the plasma density scale length. In other words: The electrons, accelerated by the laser pulse perpendicular to the critical surface, leave the plasma, stay in vacuum and bounce back into the plasma when the electromagnetic field changes its direction after half a laser cycle. In this case, the plasma wave is not resonant anymore, but rebuilt afresh each (field) cycle. This mechanism is referred to as *vacuum heating* or *Brunel absorption* and belongs, as all the

## 2 Interaction of Intense Electromagnetic Fields with Hot Dense Plasma

---

effects at higher intensities, to the collisionless absorption effects. Numerical simulation for sub-ps laser pulses and different irradiances gave up to 70% absorption for  $10^{16}$  W  $\mu\text{m}^2/\text{cm}^2$  [GB92]. Although these values might be rather theoretical and difficult to be reproduced experimentally, the simulations show a lot of interesting effects: In the vacuum heating process, typical bi-Maxwellian velocity distributions for the electrons are formed. One type of electrons therein stays within the plasma and is heated by the “not-so-resonant” plasma wave. The other type, preferably the electrons bounced back from the vacuum, achieves a much higher velocity. Their kinetic energy scales with the irradiance at about  $U_{os}=(I\lambda^2)^{1/3\dots 1/2}$  [GB92]. It should be noted, that because of the directed character of the hot electrons, the description with a “temperature” is not entirely correct and it describes their kinetic energy rather than their equilibrium statistical motion.

Another interesting feature is, that some of the electrons remain in the vacuum. These electrons build up a Coulomb field, which not only works against the motion of the other electrons in the vacuum heating process, but also accelerates any positively charged particle in the direction of the electrons. This is a first idea of how protons can be accelerated out of the plasma.

For irradiances above  $10^{18}$  W  $\mu\text{m}^2/\text{cm}^2$  not only the electron motion becomes relativistic, but also ion transport becomes significant. This has several consequences: Firstly, the mathematical treatment of the plasma has to include relativistic correction terms. Secondly, the magnetic field, neglected so far, becomes involved in the laser plasma interaction. The  $\mathbf{v}\times\mathbf{B}$  term of the Lorentz force acting on the electrons leads to an acceleration perpendicular to the electric field component. Furthermore, the so-called *ponderomotive force*, an electrostrictive force proportional to the square of the electric field component  $\mathbf{E}^2$  and directed along its gradient, presses the electrons away from maximum field amplitudes in the laser focus. The radial ponderomotive force  $\mathbf{F}_{pond}$  can be written as [KRU88], [ATT99]:

$$\mathbf{F}_{pond} = -\frac{e^2}{4m_e\omega_L^2} \nabla \mathbf{E}^2(\mathbf{r}) \quad , \quad / 2-31$$

where  $e$  and  $m_e$  are the electron’s charge and mass, respectively;  $\omega_L$  is the frequency of the electric (light) field and  $\mathbf{E}$  is its maximum amplitude<sup>1</sup>.

Thus, the ponderomotive and the Lorentz force (both containing nonlinear terms) push the electrons out of the center of the laser beam. The electrons create a charge separation, which attracts the ions they left behind. This effect is one reason for the so-called *hole boring* in the

---

<sup>1</sup> Depending on the definition of  $\mathbf{E}$  as maximum or as r.m.s. value, the formula for the ponderomotive force or the ponderomotive potential differs in various text books by a factor of 2 [HM79].

plasma. Simulations by Wilks et al. found such a behavior [WKT92]. There, ions are dragged out of the center of a laser focus ( $I_{max} = 10^{19}$  W/cm<sup>2</sup> in these calculations), leaving a hole several wavelengths deep. Another effect, supporting hole boring, comes from the enormous light pressure. It approaches 1 Gbar and exceeds the thermal plasma pressure. This presses the plasma inwards, preferentially in the focal region [GIB96]. Beside the general deformations of the hole-boring effect, the simulations of Wilks et al. showed energetic electrons as well as MeV ions behind the critical surface. There, the acceleration of the ions was explained by the light pressure. This was the first time, that ion acceleration had been shown as a direct effect of the light field. More ion acceleration mechanisms are discussed in section 2.4.

Finally, a remark concerning induced magnetic fields in the plasma should be made. The interaction of ultra-strong laser fields with the plasma causes a massive directed charge transport in the focal region. Thus, gigantic magnetic fields can appear for short times. Different mechanisms for the B-field generation have been suggested and fields of  $10^9$  G for intensities of  $10^{19}$  W/cm<sup>2</sup> were predicted (for a review see [GIB96]). Meanwhile, several experiments have been conducted, where the deflection of accelerated protons was explained by magnetic fields in the Mega Gauss range [BMB98], [NTP01], [MKS01].

### 2.3 X-Ray Emission

Typical X-ray spectra show continuous as well as discrete features (Fig. 2-5). Many different processes can contribute to X-ray emission spectra. Using a simple atomic picture for the different interactions of electrons, X-ray emissions can be sorted into three classes:

- Free-free transition

When a free electron collides with another particle it is decelerated, it loses energy and makes a transition to a lower energy free state. The excess energy is emitted as a photon. The electron changes its direction and the photon is emitted in a direction that satisfies momentum conservation. Because of its decelerating type of interaction, the radiation is called *bremstrahlung* ('braking radiation'). Due to the stochastic nature of the interaction process, bremsstrahlung spectra are continuous in their nature. Bremsstrahlung spectra from X-ray tubes typically show a maximum energy close to the cathode voltage  $U$  of the tube. Fig. 2-5 displays a bremsstrahlung spectrum from an X-ray tube with Mo anode and  $U=100$  kV.

## 2 Interaction of Intense Electromagnetic Fields with Hot Dense Plasma

- Free-bound transition

A free electron can be captured to a bound state of an ion. The excess energy will be emitted as *recombination radiation*. The emitted photons show a continuous spectrum for each bound state with a low frequency cut-off, corresponding to the minimum energy needed to remove the electron from the bound state.

- Bound-bound transition

Absorption of an energetic X-ray photon or collisions may lead to the emission from an inner shell electron of an ion or atom. This vacancy is filled by an electron of this atom (ion) from a higher energetic level. The difference in binding energy is emitted as a photon with well-defined energy. The wavelength  $\lambda$  of this radiation can be calculated using Moseley's law:

$$\frac{1}{\lambda} = R_{\infty} (Z - \sigma)^2 \cdot \left( \frac{1}{m^2} - \frac{1}{n^2} \right), \quad / 2-32$$

where  $R_{\infty}$  is Rydberg's constant,  $Z$  is the atomic number,  $\sigma$  is a shielding constant (expresses the shielding of nuclear charge by atomic electrons),  $m$  and  $n$  are the principal quantum numbers of the initial and final energetic level, respectively. Because of the discrete, well-defined character of this radiation it is also referred to as *characteristic (line) radiation*.

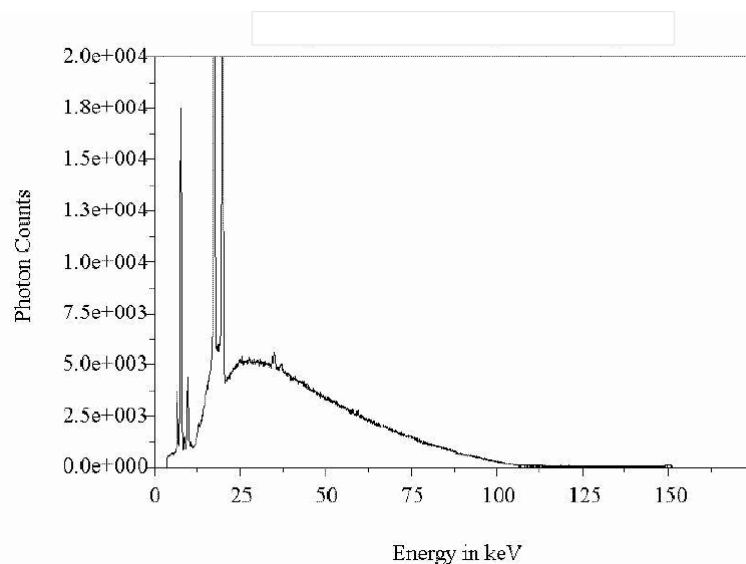


Fig. 2-5: Typical X-ray spectrum from an X-ray tube with Mo anode and  $U=100$  kV [ISU02].

The X-ray emission of a laser-produced plasma (LPP) usually contains information about the processes inside the plasma and hence, it can be used as a fingerprint for particular experimental conditions. Therefore, some remarks on emission spectra should be added to the simple classification above.

Typical spectra contain two main broadband features: The first, centered at low energies of 1 keV or less, is due to the *blackbody radiation* of the plasma. It expresses the thermal radiation of the plasma in a quasi equilibrium state. The temporal development and classification of equilibrium conditions in LPP is a broad field of discussion (see, e.g. [MB93]) beyond the scope of this work. It should be mentioned, nevertheless, that the emission of low-energy blackbody radiation of LPP starts with any (laser) pre-pulse and persists much longer than the laser pulse (until the evaporated target material thermalizes).

A different temporal signature shows the second broadband feature in LPP spectra: The bremsstrahlung from hot electrons with typical energies of tens of keV up to MeV (depending on the laser intensity) is emitted not much longer than the main laser pulse endures. While the low-energy thermal spectrum can be calculated using a Maxwellian velocity distribution, this holds only partially for the hot electrons (because of their directed non-stationary character). The emission spectrum of the hot (sometimes also referred to as *suprathermal*) electrons often appears as a high-energy trail of the emission spectrum of the thermal electrons.

Much information can be obtained from the line spectra as well. The position of the lines in the spectrum, their intensity ratio and the profile of the individual lines are determined by the plasma processes and can be investigated to understand the underlying physics. At first, the line position can be used to identify the emitting material. Beside the target, of course, this can be a part of the experimental apparatus as well as the vacuum chamber, if hot electrons hit it. If such technical problems are excluded, the line position can be used to determine the ionization state in the plasma. This can be seen in formula /2-32/, where the shielding constant  $\sigma$  changes with the numbers of electrons removed. The relation of the intensities of several of these shifted lines allows an estimation of the plasma temperature [JKM95]. In the experiments for the generation of gallium line radiation, as presented here in Chapter 4, the effect of line shifting due to ionization is negligible. There, the line radiation is assumed to be due to hot electrons hitting the cold and un-ionized target material.

The intensity ratio of two different emission lines will be exploited in the X-ray diffraction experiments described in Chapter 5. There (see section 5.3.2), the intensity ratio of two spin-

orbit split gallium K lines will be used as a means to distinguish between Ga  $K_\alpha$  and  $K_\beta$  lines without knowing the absolute energy of a measured line pair.

Other information on particular plasma parameters, such as the electron density, is obtainable from the line shape in highly resolved spectra. In a particular laser plasma experiment by Jung et al. [JKM95], the broadening of emission lines was determined. In these experiments, the broadening was identified as Stark broadening, caused by collisions of particles nearby the emitting ion. The method to obtain the electron density from the profiles of different emission lines is, of course, much more complicated than sketched here. But it shows the principal possibility to achieve information on plasma parameters from the emitted line shape.

### 2.4 Electron Acceleration in Laser-Induced Plasma Waves

In the preceding sections several mechanisms for the acceleration of electrons in a plasma by strong light fields have been discussed. These were effects that arise close to the critical surface. But already long before the light wave arrives at the region of critical density, several interactions between light and plasma particles can occur. For further understanding of this problem, the term *instability* must be examined. A light wave traveling in underdense plasma causes electrons to move leading to small differences in the electron density. Such differences are deviations from equilibrium and can cause *plasma instabilities*. This term is a very general description for many different effects in plasma physics. The most important are acoustic electron and acoustic ion waves. Instabilities can originate from the light waves but also from stochastic effects in the plasma. More about plasma instabilities can be found in many text books [ATT99], [HM79], [KRU88].

The (resonant) interaction between plasma waves and light waves can lead to the acceleration of electrons close to the velocity of light. Hence, it is important to understand the nature of such waves and the rules of their propagation in the plasma. This will be discussed in the next two subsections. Although much of the acceleration physics for electrons can be explained in this way, the ideas for ion acceleration are even more complex. Therefore, a final section will review some of the concepts published on this topic.

#### 2.4.1 Waves in Plasma

As mentioned above a light wave traveling in under-dense plasma can cause small changes in the electron density and hence, in the velocity distribution function and the local electrical field. With such an approach of small varying quantities, one can derive a longitudinal wave

equation for electron density fluctuations from the fluid plasma description, in particular the Maxwell-Euler equations /2-23/.../2-27/ [ATT99]

$$\left[ \frac{\partial^2}{\partial t^2} + \omega_p^2 - a_e^2 \nabla^2 \right] n_e(\mathbf{r}, t) = 0. \quad /2-33$$

There,  $a_e$  is the electron speed of sound ( $\gamma = 1+2/N$  is the number of degrees of freedom):

$$a_e = \left( \frac{\gamma k_B T_e}{m_e} \right)^{1/2}. \quad /2-34$$

A solution for equation /2-33/ is an appropriate electron density wave of frequency  $\omega$  and with a wave vector  $\mathbf{k}$  :

$$n_e(\mathbf{r}, t) = n_{e0} e^{-i(\omega t - \mathbf{k}\mathbf{r})}. \quad /2-35$$

Inserting this wave into the wave equation yields a dispersion relation for the *electron acoustic wave* (also referred to as *Langmuir wave*):

$$\boxed{\omega^2 = \omega_p^2 + k^2 a_e^2} \quad /2-36$$

Apparently, the wave frequency has a low-frequency cutoff at  $\omega = \omega_p$ . For small wave numbers  $k < k_D$  with  $k_D = 1/\lambda_D$ , the wavelength  $\lambda$  becomes larger than a Debye length and the fluid description works quite well. For  $k > k_D$  this changes and the influence of individual charges becomes important. The kinetic plasma description delivers an imaginary correction term for the frequency  $\omega$  that becomes effective when  $k > k_D$ . This imaginary component also reflects the damping which increases with increasing wave number.

Similarly, fluctuations in the ion density can be used to derive a wave equation for *ion-acoustic waves*. For that the equations from the fluid-plasma description have to be applied to the ion density. For a simple solution quasi-neutrality is assumed, that means  $n_{0i} = n_{0e}/Z$ , where the index zero denominates undisturbed ion and electron densities, and  $Z$  is the charge of the ions. Then, an equation for the ion density fluctuations can be derived (using ion mass  $M$ ) [ATT99]:

$$\frac{\partial^2 n_i}{\partial t^2} - \left( \frac{\gamma k_B T_i + Z\gamma k_B T_e}{M} \right) \nabla^2 n_i(\mathbf{r}, t) = 0. \quad /2-37$$

The  $T_i$  -term can be neglected, because  $T_e > T_i$ . This takes into account, that the energy is usually delivered to the electrons and transferred to the ions by collisions. Equation /2-37/ then simplifies to an *ion-acoustic wave equation*:

$$\left[ \frac{\partial^2}{\partial t^2} - a^{*2} \nabla^2 \right] n_i(\mathbf{r}, t) = 0. \quad / 2-38$$

The propagation velocity  $a^*$  here depends on the electron temperature  $T_e$  and the ion mass  $M$ :

$$a^* = \left( \frac{Z\gamma k_B T_e}{M} \right)^{1/2}. \quad / 2-39$$

That means, this low-frequency plasma oscillation is driven by the electron thermal energy, but with an inertia set by the ions with their much higher mass. Applying the usual solution of the wave equation,  $n_i(\mathbf{r}, t) = n_{i0} e^{-i(\omega t - \mathbf{k}\mathbf{r})}$  leads to a dispersion relation for the ion acoustic wave:

$$\boxed{\omega = k a^*} \quad / 2-40$$

The dispersion relations for the electron acoustic wave, for the ion acoustic wave and for transverse electromagnetic waves are shown in Fig. 2-6. This graph illustrates, that the transverse electromagnetic and the longitudinal electron-acoustic waves are high-frequency phenomena while the ion-acoustic wave is of a low-frequency nature. Therefore, on short time scales the ion-effects can be neglected again, while the electron-acoustic waves can be interesting also on the time scales of laser pulses.

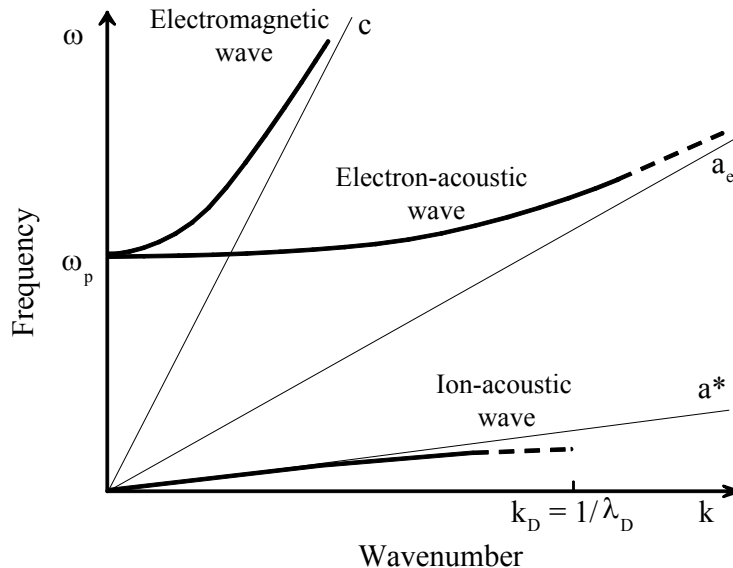


**Fig. 2-6 : Dispersion diagram for naturally occurring waves in an isotropic plasma [ATT99]. Shown are the transverse electromagnetic wave with cutoff at the plasma frequency  $\omega_p$ , a high-frequency longitudinal electron-acoustic wave and a low frequency ion-acoustic wave.**

For the transverse electromagnetic wave a similar dispersion relation can be obtained:

$$\boxed{\omega^2 = \omega_p^2 + k^2 c^2} \quad / 2-41$$

There  $\omega$  is the frequency of the wave and  $c$  is the velocity of light in vacuum. This allows a simple derivation of phase velocity  $v_\phi$  and group velocity  $v_g$  of the transversal wave ( $n_e$  and  $n_c$  are the electron density and the critical electron density, respectively):

$$v_\phi = \frac{\omega}{k} = \frac{c}{\sqrt{1 - \omega_p^2 / \omega^2}} = \frac{c}{\sqrt{1 - n_e / n_c}}, \quad / 2-42$$

$$v_g = \frac{\partial \omega}{\partial k} = c \sqrt{1 - \frac{\omega_p^2}{\omega^2}} = c \sqrt{1 - \frac{n_e}{n_c}}, \quad / 2-43$$

which, in turn, yield the relation for the real part of the refractive index  $n$ :

$$n = \sqrt{1 - \frac{\omega_p^2}{\omega^2}} = \sqrt{1 - \frac{n_e}{n_c}}. \quad / 2-44$$

Apparently, the index of refraction goes from  $n=1$  (vacuum,  $\omega_p=0$ ) to zero at the critical surface, where  $n_e=n_c$ ,  $\omega=\omega_p$ . The imaginary part of  $n$  depends on the electron–ion collision frequency and expresses the absorption of the wave in the plasma. Details can be found in plasma physics textbooks ([KRU88], [ATT99]). For more detailed treatment of plasma instabilities, one may refer to the book of Motz [HM79].

### 2.4.2 Parametric Effects, Wave Mixing and Electron Acceleration

In the Maxwell-Euler equations /2-23/.../2-27/ for the fluid–dynamical plasma description, one recognizes several product terms, such as  $n_j \mathbf{v}$ ,  $n_j \mathbf{E}$  or  $n_j (\mathbf{v} \times \mathbf{B})$ . For such terms linear superposition breaks down and they introduce the possibility of non-linear growth as well as wave mixing. Indeed, several wave mixing processes are possible in plasmas. But, as well-known from non-linear optical mixing processes, the contributing waves have to satisfy three conditions. For a typical three-wave mixing process these are:

Momentum conservation	$\hbar \mathbf{k}_0 = \hbar \mathbf{k}_1 + \hbar \mathbf{k}_2,$
Energy conservation	$\hbar \omega_0 = \hbar \omega_1 + \hbar \omega_2,$
Dispersion equations	$\varepsilon_0(\omega_0, \mathbf{k}_0) = 0 ; \quad \varepsilon_1(\omega_1, \mathbf{k}_1) = 0 ; \quad \varepsilon_2(\omega_2, \mathbf{k}_2) = 0 .$

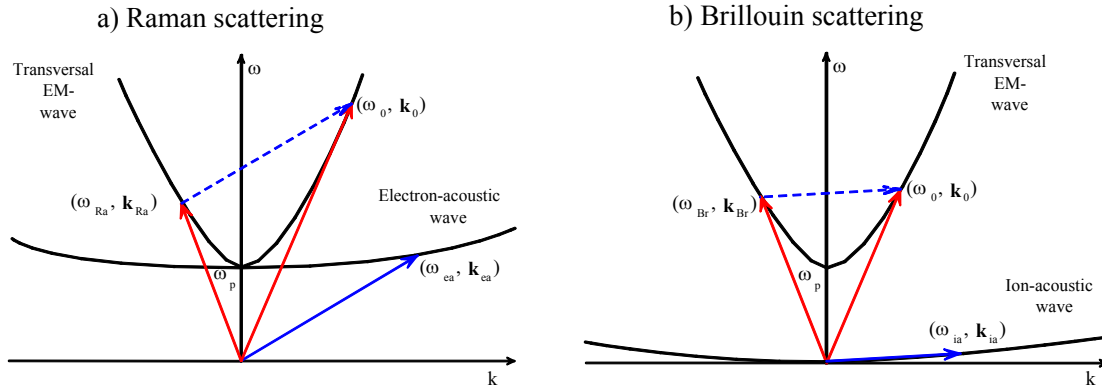


**Fig. 2-7 : Dispersion diagrams for a) Raman and b) Brillouin scattering of an incident electromagnetic (EM) wave by an electron-acoustic and ion-acoustic wave, respectively. The dashed line denotes a parallel shifted duplicate of the electron wave (ion wave) in the respective graph. It visualizes the wave matching for frequencies and wave vectors [ATT99], [HM79].**

Fig. 2-7 explains the dispersion diagrams for two simple three-wave mixing processes. The first process is the scattering of a transversal electromagnetic wave ( $t_0$ ,  $t$  for transversal) by a longitudinal electron-acoustic plasma wave ( $l_{ea}$ ,  $l$  for longitudinal). This process can be described as  $t_0 \rightarrow l_{ea} + t_{Ra}$ . The scattered wave  $t_{Ra}$  has less energy than the initial wave and the wave vector  $\mathbf{k}_{Ra}$  is opposite to the initial vector  $\mathbf{k}_0$ . Although the representation of the wave vectors is only one-dimensional, it is obvious that the scattered light is emitted backwardly. Therefore, the process is called *Raman (back-) scattering*. The scattering of electromagnetic radiation by an ion-acoustic wave is referred to as *Brillouin scattering*. In this case, the scattering wave has a low frequency and hence, the energy difference between the initial electromagnetic wave and the scattered wave is rather small. However, the direction is completely changed.

Under certain conditions (e.g. low density gradient) the scattering effects can become resonant and lead to an enormous energy transfer from the laser radiation into plasma waves. This case might be explained as follows: In a given plasma a distribution of acoustic plasma waves with parameters  $(\omega, \mathbf{k})$  already exists. Then, electromagnetic radiation with  $(\omega_0, \mathbf{k}_0)$  impinges and scatters on the plasma waves. A few plasma waves  $(\omega_1, \mathbf{k}_1)$  out of the random distribution will satisfy the conservation laws  $\hbar\mathbf{k}_0 = \hbar\mathbf{k}_1 + \hbar\mathbf{k}_2$  and  $\hbar\omega_0 = \hbar\omega_1 + \hbar\omega_2$ .

The scattered wave  $(\omega_2, \mathbf{k}_2)$  grows in amplitude and interferes with the incoming wave at a beat frequency  $\omega_0 - \omega_2$  and difference vector  $\mathbf{k}_0 - \mathbf{k}_2$ , causing the initial noise wave  $(\omega_1, \mathbf{k}_1)$  to grow in amplitude too. This process selects the waves that satisfy the energy and momentum matching conditions and let them grow out of the noise. Therefore it is called *stimulated scattering* and leads to the expressions *stimulated Raman scattering (SRS)* for the resonant

scattering on an electron-acoustic plasma wave and *stimulated Brillouin scattering (SBS)* for the respective process when an ion-acoustic wave is involved.

Particular details on plasma scattering effects, such as threshold or growth rate, were subject to various studies (experimental study [DRA92], theoretical background [HM79], [ATT99]). It is far beyond the frame of this work to go into all these details. But for the understanding of electron acceleration and some backscatter spectra presented in Chapter 6, it is helpful to discuss a few details of electron wave scattering processes.

Looking at Fig. 2-7a) it is apparent, that in the process  $t_0 \rightarrow l_{ea} + t_{Ra}$  both, the scattered Raman wave and the electron-acoustic wave, must have a frequency larger than the plasma frequency. Thus, the effect can only take place if the incident light has a frequency  $\omega_0 > 2\omega_p$ . Because the plasma frequency increases with the electron density, this condition is not satisfied beyond the plasma area where  $\omega_p$  becomes larger than  $0.5 \omega_0$ . Therefore (see equ. /2-2/ and /2-3/), the effect is limited to the pre-plasma with an electron density  $n_e < n_{crit}/4$ . However, at the *quarter-critical surface* (where  $n_e = n_{crit}/4$ ) the interaction between the light wave and the plasma wave is particularly efficient, because the plasma wave is excited at its natural resonance frequency. Driven with high amplitudes, the electron plasma wave can capture electrons within its high potential crests and accelerate them to very high energies. Attwood shows an example, where the electrons are accelerated to  $0.57c$ . Experiments [TED86] demonstrated electrons from Raman forward scattering (all k-vectors positive) with an energy  $>100$  keV together with a down-scattered  $\omega_{Ra} = \omega_0 - \omega_{ea} \approx 0.5\omega_0$  transversal wave component. Both components were emitted in forward direction. Beside the component with  $\omega_{Ra} \approx 0.5\omega_0$  some radiation with  $\frac{3}{2}\omega_0$  was observed. This spectral component can appear when a plasma wave with  $\omega_{ea} \approx 0.5\omega_0$  recombines with the laser light.

This effect is also known as a secondary process after a so-called *two plasmon decay (TPD)*. For the term TPD a quantum-mechanical approach is required and the (quantized) electron plasma oscillations are denoted as *plasmons* [HM79]. The process of TPD is a decay of one photon into two plasmons  $t_0 \rightarrow l_{p1} + l_{p2}$ . Fig. 2-8 a) illustrates the wave matching conditions for this process. In Fig. 2-8 b) the recombination process is illustrated, which can lead to radiation with  $3/2 \omega_0$  ( $\omega_0$  laser frequency) after a two-plasmon decay. In this process a plasma wave with  $\omega_{ea} \approx 0.5\omega_0$  (from TPD or other processes) mixes with the (reflected) laser wave to a new transversal electromagnetic wave with  $\omega = \omega_{ea} + \omega_0 \approx 1.5\omega_0$ . Experimental aspects of this radiation will be discussed in more detail in Chapter 6.

## 2 Interaction of Intense Electromagnetic Fields with Hot Dense Plasma

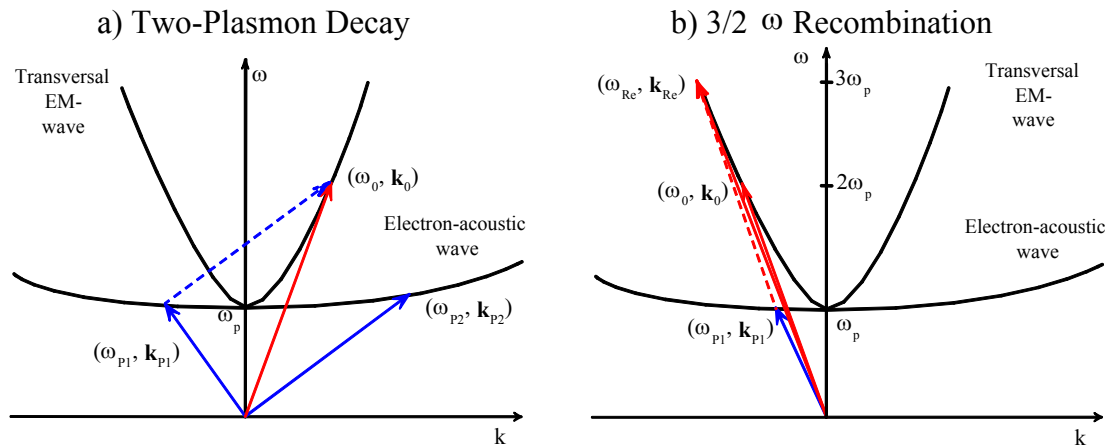


**Fig. 2-8 : Dispersion diagrams illustrating a) two-plasmon decay and b) the recombination of a plasmon with a reflected light wave to create  $3/2 \omega_0$  radiation. The dashed lines are shifted duplicates of one participating vector and visualize the wave matching.**

Summarizing, two basic classes of electron acceleration mechanisms in plasmas have been introduced:

- 1) Direct acceleration in the electromagnetic field close to the critical surface. Due to many different absorption processes, the electrons can be accelerated to energies far above the thermal average of the plasma. Some of these processes (resonance absorption) are resonant and can transfer a large part of the laser energy into “hot electrons”. These mechanisms become particularly efficient for hot dense plasmas with steep density gradients, as produced with strong sub-ps laser pulses.
- 2) Acceleration in resonant parametric wave mixing processes. By a resonant interaction between the incident light wave and electron-acoustic plasma waves (plasmon), a large fraction of energy can be transferred into the wave and captured electrons can be accelerated to relativistic energies. These processes need a longer interaction for energy transfer and therefore a low electron density gradient. They have highest efficiency in the vicinity of the quarter critical (density) surface.

A combination of short laser pulses and a plasma wave interaction is the *electron wakefield accelerator* as suggested by Tajima and Dawson. [TD79] Their concept focuses on the direct excitation of a plasma wave by the ponderomotive force of a traveling light wave or by using the beat frequency of two lasers, detuned by the plasmon frequency. In a more recent publication by Umstadter [UMS01], a distinction is made between the self-modulated laser

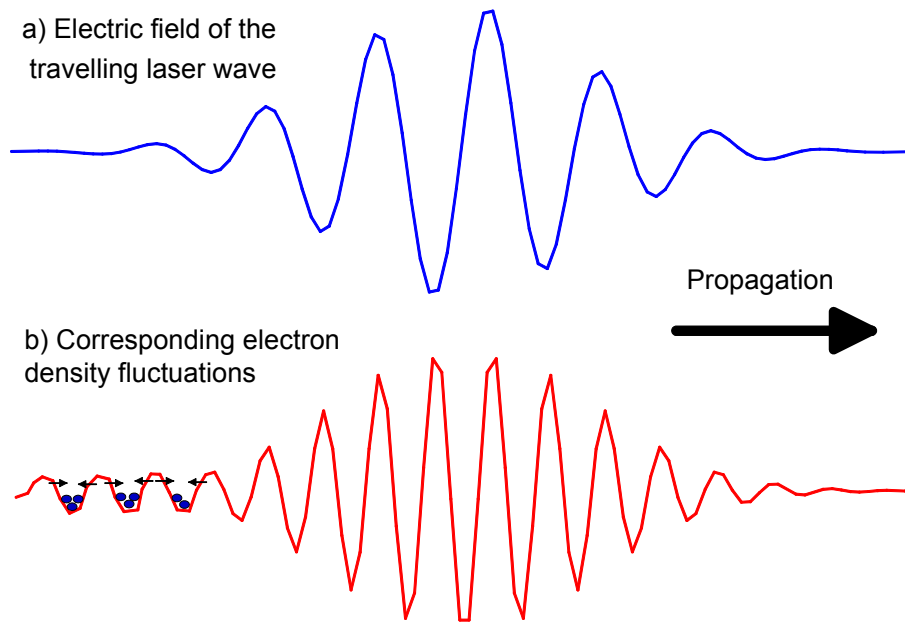


**Fig. 2-9 : Schematic illustration of wake-field acceleration. Little arrows denote Coulomb forces acting on electrons captured in the potential of the density fluctuations**

wakefield accelerator (SMLWFA) and the laser wakefield accelerator (LWFA). The first is simply another name for stimulated forward Raman scattering. The idea of the wakefield accelerator can be explained as follows (Fig. 2-9): When the laser pulse passes the plasma, it creates density fluctuations by pressing electrons away from the locations of maximum electrical field. These fluctuations remain after the field has almost gone and form a longitudinal wave, traveling directly behind the laser pulse with a comparable velocity. If this wave stays in phase with the laser pulse (like the wake behind a boat), it can trap electrons and accelerate them to the velocity of the light pulse. For efficient energy transfer this method requires long path lengths in low density low gradient plasma (typically in gas jets at  $0.01n_{\text{crit}}$  or less [SNC01], [SLF96]). Therefore, the wakefield accelerator belongs to the second class of acceleration mechanisms listed above.

A comparison of results of both classes of acceleration mechanisms led to a surprising result [SAN01]: The wave interactions (second class of effects) yield the “hotter” electrons with less laser intensity. The explanation, that this effect is due to the much longer interaction lengths in the case of parametric wave interactions, seems intriguing. For the scope of the experiments presented here, it should be noted that wave effects can accelerate electrons to energies as high or higher than predicted from estimates based on effects near the critical surface only. It agrees with the fact proven many times, that X-ray generation with a preformed plasma is much more efficient than with a steep gradient only [TF99].

### 2.5 Ion Acceleration in Ultra-Strong Laser Fields

The results of early investigations on accelerated ions have been collected in a review paper by Gitomer et al. [GJB86]. Experiments were done with various laser systems with a power of up to  $10^{17}$  W/cm<sup>2</sup>. The targets were solids in most cases. Accelerated ions were found as an unwanted side effect and identified as potential problem for laser fusion experiments. The ions were identified as hydrogen (from vacuum pump oil) and copper, carbon, nitrogen and oxygen from other vacuum contaminants. In experimental as well as numerical analysis a strong correlation was found between the ion energy and hot electron-temperature. Gitomer et al. already presented five different models to explain the ion acceleration effects. Among them were plasma streaming effects, transport due to ponderomotive forces as well as due to Coulomb forces.

With the advent of ultra-strong sub-ps lasers (focal intensities above  $10^{18}$  W/cm<sup>2</sup>) in the 1990s a new series of proton-acceleration experiments started ([FNB94], [BBD97], [CKD00], [MGF00], [SKH00], [HBC00]). Subsequently, protons attracted much more attention and many new applications for MeV protons were suggested. (e.g. table-top nuclid [SZB00] or neutron [PSP98] production, proton-based ICF [RCK01]) First of all, more research was done to improve the understanding of the ion-acceleration processes. A stream of relativistic electrons from the laser focal region through the target was identified as a primary process for ion acceleration. But the consecutive processes turned out to be much more complicated. Zepf et al. [ZCK01] identified fields in three separate regions of thin-foil targets that can be involved in ion acceleration (see Fig. 2-10):

- 1) Near the critical density. In the laser focal region ions are accelerated by ponderomotive forces as part of the hole boring effect.
- 2) Inside the target. In the solid-density plasma fast electrons propagate towards the rear side of the target. The electron current induces a magnetic field which, in turn induces a strong axial electric field.
- 3) Behind the target. There, the electrons set up strong space-charge fields (*electron sheath*). The field is expected to scale with the hot-electron temperature.

A number of remarks should be added to this still simplified picture. First, the physics described above is derived from experiments at  $10^{19}$  ...  $10^{20}$  W/cm<sup>2</sup> laser intensity (with the VULCAN laser at Rutherford Appleton Laboratory, Chilton, GB). Most of the accelerated ions were stripped hydrogen atoms, i.e. protons. The observed protons have energies up to

about 40 MeV. Simulations for the effect of the fields mentioned yield only a few MeV proton energy gain for each region. [ZCK01] This is much less than observed in the experiments. Furthermore it should be mentioned, that, although most protons were accelerated in forward

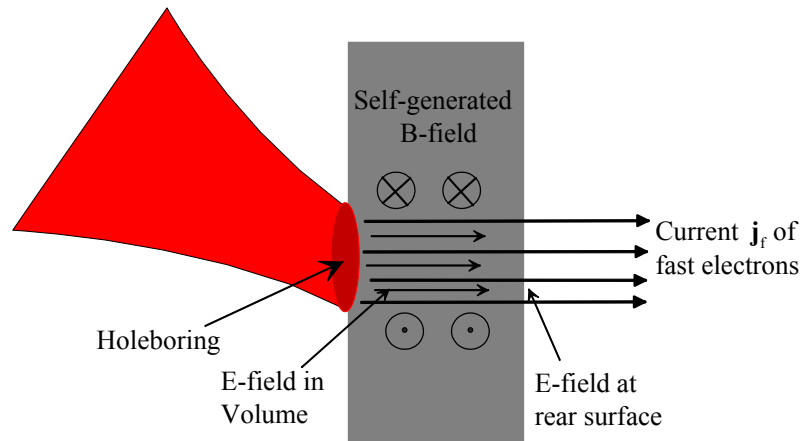


**Fig. 2-10 : Schematic of the plasma interaction and the fields therein following Zepf et al. [ZCK01]**

direction (i.e. through the target), a remarkable fraction was backscattered. This might be explained by a space-charge effect due to electrons expelled from the target surface.

In the conclusions of their investigations, Zepf et al. admit that there are difficulties to identify unambiguously a dominant acceleration process. In particular, the origin of the high-energy protons could not be verified completely. This points to an interesting discussion in the scientific community, in particular between the groups at RAL and LLNL, about the acceleration mechanisms. While the experiments at RAL ([CKD00], [CKZ00]) and at the CUOS at the University of Michigan ([MGF00],[NMB01]) implied the proton origin in the target or on its front side, experiments using a wedged target at LLNL proved the proton origin from the target's rear side [HBC00]. In particular, the experiments of Nemoto et al. [NMB01] with a deuterated polystyrene layer on the front side gave evidence of the front-side origin of the (deuterium) ions.

The contradiction is not resolved yet, but a recent publication from the LLNL group gave a new impetus. MacKinnon et al. [MSP02] found a strong dependence of the proton energy yield on the target thickness and explained that with a hot-electron recirculation. The theoretical model works as follows: First, electrons are accelerated through the target by the  $\mathbf{J} \times \mathbf{B}$  force. Behind the target they form an electron sheath (often called *Debye sheath*) which reflects the consecutive electrons back to the targets front side. If the laser pulse is long

## **2 Interaction of Intense Electromagnetic Fields with Hot Dense Plasma**

---

enough, an electron sheath is kept at the front surface too. Here, the electrons from the backside are reflected again. Arriving at the backside they increase the electron density there. In the model of Mackinnon et al.(and also in the previous models of the LLNL group) this electron density at the backside creates the crucial electrical field for the proton acceleration. If now the time for recirculation of the electrons (15 fs for one electron transit in a 5  $\mu\text{m}$  Al foil) exceeds the laser pulse duration, the recirculation stops and the electron density at the back surface drops down. This behavior could be reproduced in experiments where the maximum proton energy decreased with increasing target thickness much more than one could explain with simple deceleration in the material. In particular, the behavior changed at a target thickness where the double electron-transit time corresponds to the laser pulse duration.

Summarizing, it can be stated, that , mostly, ion acceleration in plasmas is seen as a secondary effect of the electron acceleration. In all ion acceleration experiments energetic electrons were observed and accounted as a primary effect. Several forces contributing to the production of energetic ions were suggested but the precise mechanisms and their relative importance are still subject to scientific investigation. It should be mentioned that simulation prove the primary role of electrons for intensities of  $10^{19}$  W/cm<sup>2</sup> [AP01], but for the case of ultra-strong fields at  $10^{21}$  W/cm<sup>2</sup> a direct acceleration of protons by the light field was suggested [RBC01].

Nevertheless, laser induced generation of energetic ions has become an established technology (not only in the large-scale facilities) and several applications of MeV protons are now becoming reality (e.g. plasma diagnosis [BSC01]).